

Yang Li

Quarkonium wave functions on the light front

December 6, 2016

Abstract We study heavy quarkonium within the light-front Hamiltonian formalism. Our effective Hamiltonian is based on the holographic QCD confining potential and the one-gluon exchange interaction with a running coupling. The obtained spectra are compared with experimental measurements. We present a set of light-front wave functions, which exhibit rich structure and are consistent with the nonrelativistic picture. Finally, we use the wave functions to compute the charge and mass radii.

Keywords light front · wave function · heavy quarkonium · holography · radius

1 Introduction

The light-front Hamiltonian approach is poised as a unique tool to understand the non-perturbative dynamics of quantum field theory in Minkowski space-time [1]. The Hamiltonian formalism provides frame-independent wave functions that are essential for understanding the underlying structure of relativistic bound state systems. The obtained light-front wave functions (LFWFs) can be used to compute hadronic observables and distributions defined in the infinite momentum frame (IMF), and to study exclusive processes in the deep inelastic scattering (DIS), which are otherwise not easily accessible in other methods [2]. Therefore, the light-front Hamiltonian approach is complementary to Lagrangian methods formulated in Euclidean space, e.g., lattice gauge theory.

Recently we proposed a phenomenological light-front potential model for mesons based on light-front holography [3]. We applied this model to charmonium and bottomonium, and solved the system in a basis function representation. The obtained mass spectra, form factors and decay constants are compared with experiments and other established methods. The LFWFs are also used to study exclusive vector meson productions in DIS [4]. Very recently, similar work has been done within the Dyson-Schwinger/Bethe-Salpeter approach [5] and the covariant spectator theory (CST) [6].

In this paper, we propose an improvement of the model in Ref. [3] by incorporating the evolution of the coupling based on perturbative QCD (pQCD). We will show that the mass spectra are improved. Another aim of this paper is to display the LFWFs, which reveal first-hand information of the hadrons, and also help to visualize relativistic bound states on the light front. Heavy quarkonium is an ideal system to explore LFWFs, as the characteristic heavy quark velocities are small [$v \sim (0.1-0.3)$] compared to the speed of light and the familiar nonrelativistic quantum mechanical language and intuition may be applied.

Yang Li
Department of Physics and Astronomy, Iowa State University, Ames, IA 50011, USA
E-mail: leeyoung@iastate.edu

2 Formalism

The effective Hamiltonian for the model reads [3],

$$H_{\text{eff}} = \frac{\mathbf{k}_\perp^2 + m_q^2}{x} + \frac{\mathbf{k}_\perp^2 + m_{\bar{q}}^2}{1-x} + \kappa^4 \zeta_\perp^2 - \frac{\kappa^4}{(m_q + m_{\bar{q}})^2} \partial_x (x(1-x) \partial_x) - \frac{C_F 4\pi\alpha_s(Q^2)}{Q^2} \bar{u}_{s'}(k') \gamma_\mu u_s(k) \bar{v}_{\bar{s}}(\bar{k}) \gamma^\mu v_{\bar{s}'}(\bar{k}'). \quad (1)$$

where $Q^2 = -\bar{q}^2 = -(1/2)(k' - k)^2 - (1/2)(\bar{k}' - \bar{k})^2$ is the average 4-momentum squared carried by the exchanged gluon. The confining term $\kappa^4 \zeta_\perp^2$ comes from the “soft-wall” light-front holography, κ is the strength of the confinement, and $\zeta_\perp \equiv \sqrt{x(1-x)} \mathbf{r}_\perp$ is Brodsky and de Téramond’s holographic variable [7]. ζ_\perp and x are taken as the independent variables, $\partial_x f(x, \zeta_\perp) = \partial f(x, \zeta_\perp) / \partial x|_{\zeta_\perp}$. $C_F = (N_c^2 - 1)/(2N_c) = 4/3$ is the color factor. m_q ($m_{\bar{q}}$) is the mass of the quark (anti-quark). The longitudinal confinement comes from completing the transverse holographic confinement in the finite mass case and is consistent with the pQCD asymptotics of the distribution amplitude $x^\beta(1-x)^\alpha$. The longitudinal confining strength is fixed in the nonrelativistic limit hence no additional parameter is introduced.

In Ref. [3], the strong coupling α_s is assumed fixed for each system, say, charmonium, whereas for different systems, the values of α_s are different and are related through the pQCD evolution. While such treatment is reasonable (indeed traditional, see e.g. [8]), as the mass difference between states in the same system, e.g. J/ψ and $\psi(2S)$, is small compared to their respective masses, nevertheless, the inclusion of the running coupling implements important QCD physics. Another motivation is to improve the rotational symmetry and the hyperfine structure. In the effective one-gluon exchange kernel, [9–11], a non-covariant UV counterterm is introduced to regularize the UV divergence appearing in the box diagram [9; 12], which further spoils the rotational symmetry as will be seen in the mass spectra below. The introduction of the running coupling changes the UV asymptotics of the one-gluon exchange kernel¹. As a result, the counterterm is not necessary anymore. While rotational symmetry is not fully restored, as we will see, the breaking of rotational symmetry is moderated, and the hyperfine structure is significantly improved.

In the effective one-gluon exchange interaction Eq. (1), the 4-momentum squared of the exchanged gluon Q^2 naturally appears. The running coupling can be introduced as a function of Q^2 :

$$\alpha_s(Q^2) = \frac{\alpha_s(M_Z^2)}{1 + \alpha_s(M_Z^2) \beta_0 \ln(\mu_{\text{IR}}^2 + Q^2)/(\mu_{\text{IR}}^2 + M_Z^2)}. \quad (2)$$

where $N_f = 4$ for charmonium and $N_f = 5$ for bottomonium. Here μ_{IR} is an IR cutoff introduced to avoid the pQCD IR catastrophe. Similar forms are used in the literature, e.g. Ref. [13]. In practice, we choose $\alpha_s(0) = 0.6$. We find the spectrum is not sensitive for the choice of $\alpha_s(0)$ within the range $0.4 \leq \alpha_s(0) \leq 0.8$.

The state vectors, hence the LFWFs, are obtained from diagonalizing the Light Cone Hamiltonian operator $\hat{H}_{\text{LC}} \equiv P^+ \hat{P}^- - \mathbf{P}_\perp^2$:

$$H_{\text{LC}} |\psi_h(P^+, \mathbf{P}_\perp, j, m_j)\rangle = M_h^2 |\psi_h(P^+, \mathbf{P}_\perp, j, m_j)\rangle. \quad (3)$$

The state vectors can be represented in the Fock space:

$$|\psi_h(P^+, \mathbf{P}_\perp, j, m_j)\rangle = \sum_{s, \bar{s}} \int_0^1 \frac{dx}{2x(1-x)} \int \frac{d^2 \mathbf{k}_\perp}{(2\pi)^3} \psi_{s\bar{s}/h}^{(m_j)}(\mathbf{k}_\perp, x) \times \frac{1}{\sqrt{N_c}} \sum_{i=1}^{N_c} b_{si}^\dagger(xP^+, \mathbf{k}_\perp + x\mathbf{P}_\perp) d_{\bar{s}i}^\dagger((1-x)P^+, -\mathbf{k}_\perp + (1-x)\mathbf{P}_\perp) |0\rangle. \quad (4)$$

¹ This is not to say, however, that now the UV asymptotics of the one-gluon exchange kernel is consistent with the perturbation theory. But the UV asymptotics is not easily studied in the basis representation and the investigation of the UV asymptotics is beyond the scope of this paper.

Table 1 Summary of the model parameters. μ_g is the gluon mass, used to regularize the integrable Coulomb singularity. $\langle M_{\text{cal}} - M_{\text{pdg}} \rangle$ represents the r.m.s. deviation of the masses from the Particle Data Group values for states below the threshold. $\langle \delta M_{m_j} \rangle$ represents the r.m.s. value of the mass spreads for the same state with different magnetic projection m_j 's.

	N_f	μ_g (GeV)	κ (GeV)	m_q (GeV)	$\langle M_{\text{cal}} - M_{\text{pdg}} \rangle$	$\langle \delta M_{m_j} \rangle$	# states	$N_{\text{max}} = L_{\text{max}}$
$c\bar{c}$	4	0.02	0.985	1.570	41 MeV	15 MeV	8 states	8
			0.979	1.587	32	21		16
			0.972	1.596	31	17		24
			0.966	1.603	31	17		32
$b\bar{b}$	5	0.02	1.387	4.894	48 MeV	6 MeV	14 states	8
			1.392	4.899	41	6		16
			1.390	4.901	39	6		24
			1.389	4.902	38	8		32

Here j and m_j are the intrinsic spin and the spin projection of the particle. The coefficient of the expansion, $\psi_{s\bar{s}/h}^{(m_j)}(\mathbf{k}_\perp, x)$, is the (two-body) LFWF, which is normalized as,

$$\sum_{s, \bar{s}} \int_0^1 \frac{dx}{2x(1-x)} \int \frac{d^2 \mathbf{k}_\perp}{(2\pi)^3} \psi_{s\bar{s}/h'}^{(m'_j)*}(\mathbf{k}_\perp, x) \psi_{s\bar{s}/h}^{(m_j)}(\mathbf{k}_\perp, x) = \delta_{hh'} \delta_{m_j, m'_j}. \quad (5)$$

It is useful to introduce LFWFs in the transverse coordinate space:

$$\tilde{\psi}_{s\bar{s}}(\mathbf{r}_\perp, x) \equiv \frac{1}{\sqrt{x(1-x)}} \int \frac{d^2 k_\perp}{(2\pi)^2} e^{i\mathbf{k}_\perp \cdot \mathbf{r}_\perp} \psi_{s\bar{s}}(\mathbf{k}_\perp, x). \quad (6)$$

Following Ref. [3], the effective Hamiltonian Eq. (1) was solved in a basis function approach. The LFWFs then are represented as,

$$\begin{aligned} \psi_{ss'/h}(\mathbf{k}_\perp, x) &= \sum_{n, m, l} \psi_h(n, m, l, s, s') \phi_{nm}(\mathbf{k}_\perp / \sqrt{x(1-x)}) \chi_l(x); \\ \tilde{\psi}_{ss'/h}(\mathbf{r}_\perp, x) &= \sqrt{x(1-x)} \sum_{n, m, l} \psi_h(n, m, l, s, s') \tilde{\phi}_{nm}(\sqrt{x(1-x)} \mathbf{r}_\perp) \chi_l(x). \end{aligned} \quad (7)$$

Here the coefficients $\psi_h(n, m, l, s, s')$ are obtained from diagonalization. Basis function ϕ_{nm} and χ_l are the solutions of the Hamiltonian without the one-gluon exchange interaction, i.e., the kinetic energy plus the confinement terms. Specifically, $\tilde{\phi}_{nm}(\boldsymbol{\zeta}_\perp)$ is the harmonic oscillator function in the holographic variables. $\chi_l(x)$ is the Jacobi polynomials weighed by $x^{\frac{\beta}{2}}(1-x)^{\frac{\alpha}{2}}$, where $\alpha = 2m_{\bar{q}}(m_q + m_{\bar{q}})/\kappa^2$, $\beta = 2m_q(m_q + m_{\bar{q}})/\kappa^2$.

In practical calculations, the basis is truncated and LFWFs have a corresponding finite set of terms in Eqs. (7). Observables are evaluated from finite-dimensional representations and, in principle, have to be extrapolated to the complete basis. Following Ref. [3], the basis are truncated according to:

$$2n + |m| + 1 \leq N_{\text{max}}, \quad 0 \leq l \leq L_{\text{max}}. \quad (8)$$

3 Results

The model parameters are summarized in Table 1. In particular, the confining strength κ and the effective quark mass m_q are obtained from fitting to the PDG mass spectrum below the continuum thresholds. The reconstructed charmonium and bottomonium spectra are shown in Fig. 1. The r.m.s. deviation of the masses from the PDG values are 31 MeV and 38 MeV for charmonia and bottomonia below the thresholds, respectively. These r.m.s. deviations are significantly reduced ($\sim 50\%$ for charmonium, $\sim 25\%$ for bottomonium) from the fixed coupling results reported in Ref. [3]. Our spectroscopy is competitive with those obtained from other methods, e.g. [5; 6; 14]. Not only are the mass eigenvalues improved, their dependence on m_j , an indicator for the violation of the rotational symmetry, is also

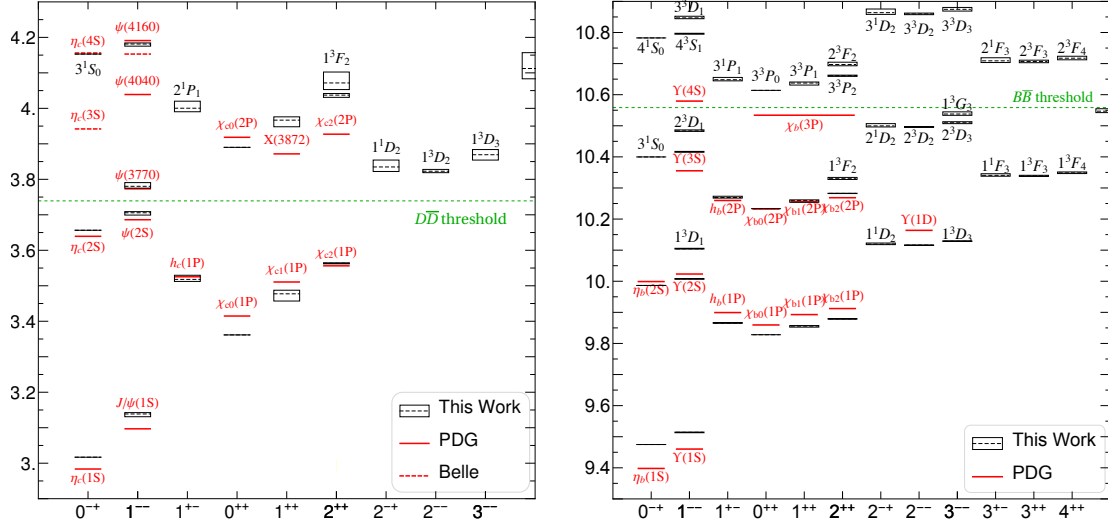


Fig. 1 The reconstructed charmonium (*left*) and bottomonium (*right*) spectra at $N_{\max} = L_{\max} = 32$. The horizontal axes marks the quantum numbers J^{PC} . The vertical axes marks the mass eigenvalues in GeV. The parameters are listed in Table 1. The r.m.s. deviation of the masses from the PDG values are 31 MeV and 38 MeV for charmonium and bottomonium, respectively. The mean mass spreads, i.e. the mean heights of the boxes, are 17 MeV and 8 MeV for charmonium and bottomonium, respectively.

weakened. For example, the mean mass spreads, i.e. the mean heights of the boxes in Fig. 1, are 17 MeV and 8 MeV for charmonia and bottomonia below the thresholds, respectively.

Wave functions provide full information of the system. Despite of their significance in hadron physics, LFWFs, especially those of the excited states, are rarely found in the literature (cf. [15]). We present representative charmonium LFWFs in Figs. 2–4.

Figure 2 shows the coordinate space LFWFs for vector meson J/ψ . For each spin alignment, the orbital angular momentum projection $m_\ell = \lambda - s_1 - s_2$ is definite ($\lambda \equiv m_j$). Hereafter, we drop the global phases $\exp(im_\ell\theta)$ related to the orbital angular momentum, while retaining the relative sign for negative values of r_\perp . It is apparent that $\psi_{\uparrow\downarrow\uparrow\downarrow}^{\lambda=0}$ [Fig. 2(a)] and $\psi_{\uparrow\uparrow}^{\lambda=+1}$ [Fig. 2(d)] are the leading LFWFs for polarization $\lambda = 0$ and $\lambda = +1$, respectively. And they are almost identical in magnitude. Thus the nonrelativistic picture emerges that J/ψ is an S -wave in direct product with a triplet spin configuration. Subleading LFWFs also exist [Figs. 2(b), 2(c), 2(e), 2(f)] due to relativity. For example, $\psi_{\downarrow\downarrow}^{\lambda=+1}$ [Fig. 2(f)] resembles a D -wave function ($\ell = 2, m_\ell = 2$), as a result of the S - D mixing.

Figure 3 compares the leading components of the vector meson J/ψ with its “radial” excitation $\psi(2S)$ and “angular” excitation $\psi(1D)$. Rich details emerge in the excited states. The $\psi(2S)$ LFWFs show nodes in both the transverse radial direction (r_\perp) and the longitudinal direction (x), consistent with the nonrelativistic interpretation, where the radial excitation is homogeneous in all 3 directions. LFWFs on the top panel (bottom panel) are with the polarization $\lambda = 0$ ($\lambda = +1$). While the leading components of a S -wave vector meson, e.g., J/ψ and $\psi(2S)$, for the all polarizations are almost identical [Fig. 3(a) vs 3(d) and Fig. 3(b) vs 3(e)], those of the D -wave vector meson $\psi(1D)$ are dramatically different [Fig. 3(c) vs 3(f)]. However, this is consistent with the nonrelativistic picture that the wave function is dominated by the D -wave ($\ell = 2$). It is easy to see that the leading components of $\psi(1D)$ are $\psi_{\uparrow\downarrow\uparrow\downarrow}^{\lambda=0}(\mathbf{r}_\perp, x)$ ($m_\ell = 0$) and $\psi_{\downarrow\downarrow}^{\lambda=+1}(\mathbf{r}_\perp, x)$ ($m_\ell = 2$). The apparent difference between the two polarizations in fact resembles the difference between the D -wave spherical harmonics $Y_2^0(\hat{r})$ and $Y_2^2(\hat{r})$.

Figure 4 presents the LFWFs of $\eta_c(3S)$. The wave functions for this highly excited state reveal complicated inner structure. The leading components $\psi_{\uparrow\downarrow\uparrow\downarrow}^{\lambda=0}(\mathbf{r}_\perp, x)$ has two nodes and is presumably dominated by a $3S$ -wave. The subleading LFWF $\psi_{\downarrow\downarrow}^{\lambda=0}(\mathbf{r}_\perp, x)$ may contain both radial and radial excitations and exhibits a nesting quadruple pattern.

Another way of visualizing relativistic bound states, in connection with the experiments, is to use the impact parameter generalized parton distributions (GPDs) [16]. These quantities are closely related to the LFWFs [17]. In fact, they are just the squared LFWFs in the coordinate space, inserting gauge

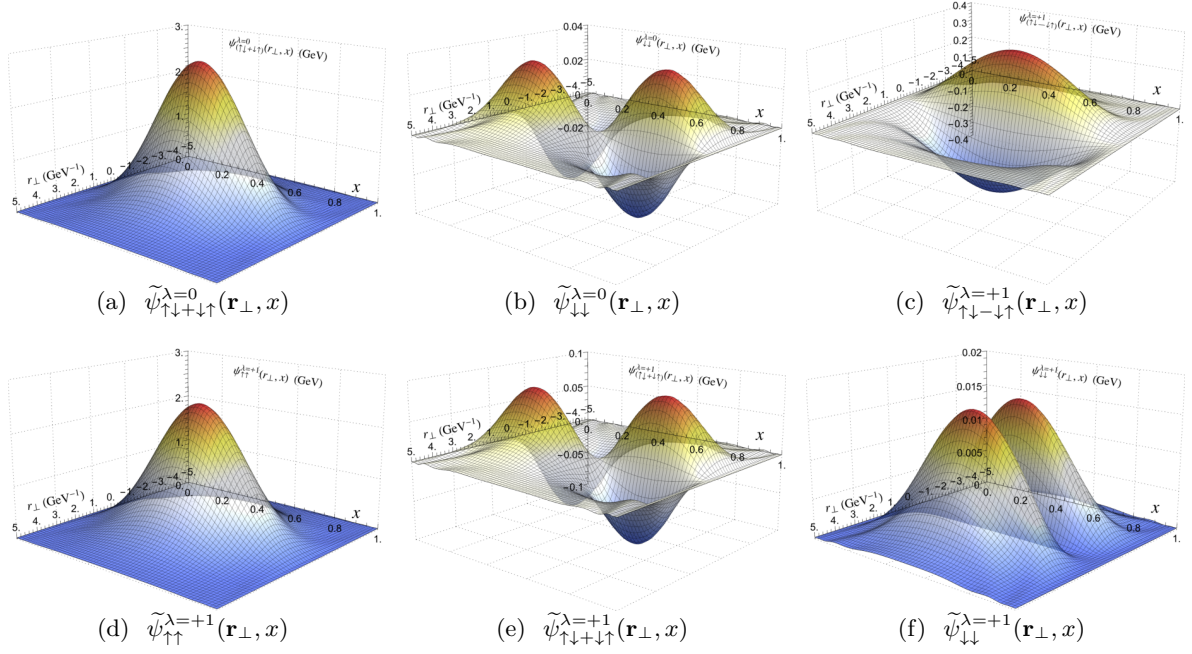


Fig. 2 (Color online) The J/ψ LFWFs plotted in 3D for polarizations $\lambda = 0$ (a-b), and $\lambda = +1$ (c-f), for various spin alignments.

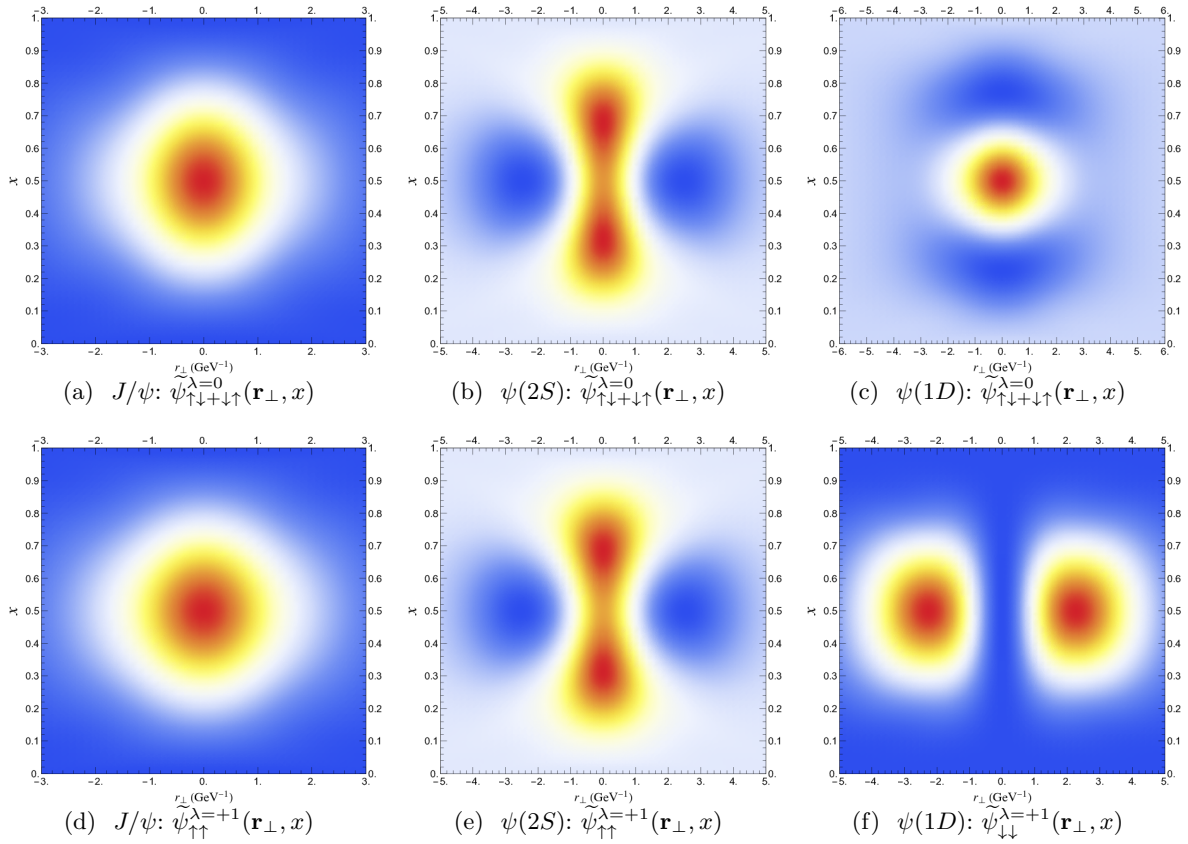


Fig. 3 (Color online) Leading components of the vector meson J/ψ and its radial excitation $\psi(2S)$ and angular excitation $\psi(1D)$ for polarization $\lambda = 0$ (a-c) and $\lambda = +1$ (d-f). The color scheme is the same as Fig. 2.

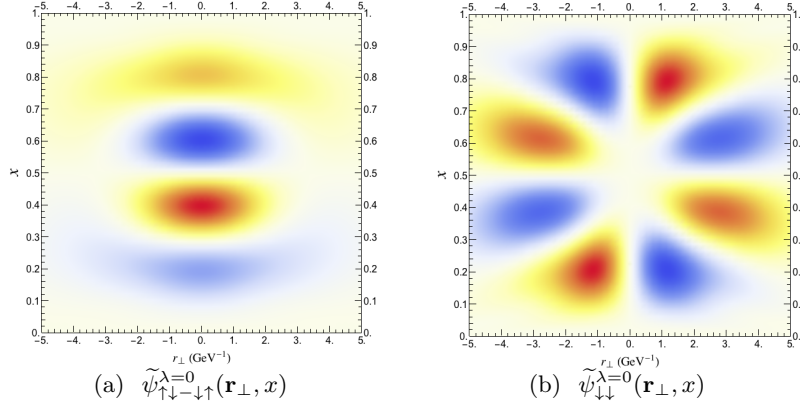


Fig. 4 (Color online) LFWFs of $\eta_c(3S)$. The color scheme is the same as Fig. 2.

Table 2 The r.m.s. charge and the mass radii of charmonia and bottomonia. Results are extrapolated from $N_{\max} = 8, 16, 24, 32$. Numerical uncertainties are estimated from the difference between the extrapolated values and the $N_{\max} = 32$ values.

(fm)	η_c	χ_{c0}	$\eta_c(2S)$	η_b	χ_{b0}	$\eta_b(2S)$	$\chi_{b0}(2P)$	$\eta_b(3S)$
charge	0.165(7)	0.231(7)	0.3468(8)	0.109(1)	0.175(3)	0.2235(4)	0.267(3)	0.306(2)
mass	0.150(6)	0.209(6)	0.332(2)	0.107(4)	0.171(1)	0.221(2)	0.263(1)	0.302(2)

links as necessary. The impact parameter GPDs for a similar system—positronium—have been shown in Ref. [18].

4 Charge and Mass Radii

We use the LFWFs to study the the root-mean squared (r.m.s.) charge and the mass radii. In relativistic dynamics, the r.m.s. radii are defined from the corresponding form factors (electromagnetic form factor F_c and the gravitational form factor F_g) which in turn are related to the hadron matrix elements of conserved currents (electromagnetic current J^μ and the energy-momentum tensor $T^{\mu\nu}$):

$$\langle r_c^2 \rangle \equiv -6 \frac{\partial}{\partial q^2} F_c(q^2) \Big|_{q \rightarrow 0}, \quad \langle r_m^2 \rangle \equiv -6 \frac{\partial}{\partial q^2} F_g(q^2) \Big|_{q \rightarrow 0}. \quad (9)$$

For the charge form factor, we only couple the probing photon to the quark. In light-front dynamics, it can be shown (see Appedix A) that the r.m.s. radii are related to the impact parameter $\mathbf{b}_\perp \equiv (1-x)\mathbf{r}_\perp$ [16] and the holographic variable $\zeta_\perp \equiv \sqrt{x(1-x)}\mathbf{r}_\perp$ [7]:

$$\langle r_c^2 \rangle = \frac{3}{2} \sum_{s,s'} \int_0^1 \frac{dx}{4\pi} \int d^2 r_\perp (1-x)^2 \mathbf{r}_\perp^2 \tilde{\psi}_{ss'/h}^{(\lambda)*}(\mathbf{r}_\perp, x) \tilde{\psi}_{ss'/h}^{(\lambda)}(\mathbf{r}_\perp, x) \equiv \frac{3}{2} \langle \mathbf{b}_\perp^2 \rangle; \quad (10)$$

$$\langle r_m^2 \rangle = \frac{3}{2} \sum_{s,s'} \int_0^1 \frac{dx}{4\pi} \int d^2 r_\perp x(1-x) \mathbf{r}_\perp^2 \tilde{\psi}_{ss'/h}^{(\lambda)*}(\mathbf{r}_\perp, x) \tilde{\psi}_{ss'/h}^{(\lambda)}(\mathbf{r}_\perp, x) \equiv \frac{3}{2} \langle \zeta_\perp^2 \rangle. \quad (11)$$

The results are summarized in Table 2. Note that the difference between $\langle r_c^2 \rangle$ and $\langle r_m^2 \rangle$ is a relativistic effect.

5 Summary and Outlook

The light-front Hamiltonian formalism provides a natural framework to understand strongly interacting relativistic bound states. We demonstrate this in a model that implements a holographic confinement

and a one-gluon exchange interaction in the heavy quarkonium systems. We update the previous results by incorporating the evolution of the strong interaction coupling constant. The resulting spectroscopy is compared favorably with the experiments. We present the wave functions, which bridge the nonrelativistic picture and the quantum field theoretical treatment of heavy quarkonium. They offer a unique way to visualize and to understand the structure of the relativistic bound states.

Our model can be applied to other mesons, e.g., heavy-light and light mesons, which is in progress. Another important improvement is to include the self-energy correction [20; 21], which will allow us to go beyond the light-front potential model treatment and to build a consistent effective light-front model for hadrons.

There are several promising ways under development to go beyond the current phenomenological model. The first one is the systematic Fock sector expansion with a non-perturbative sector dependent renormalization [22; 23]. The second one is the full configuration interaction simulation, with or without the coupled cluster technique, of the light-front QCD Hamiltonian within the basis function approach [24]. The third line of investigation is to use the effective Hamiltonians obtained from a similarity renormalization group with a systematic perturbative expansion [25]. Last but not least, progress in the holographic approach to QCD may also provide new insights. The current model can be linked to all these lines of investigation. The physics learned from the current model, and the techniques employed in our model, may be helpful to explore those more ambitious approaches.

Acknowledgements I wish to thank the organizers of the Light Cone 2016 conference. I acknowledge valuable discussions with J.P. Vary, P. Maris, K. Tuchin, S.J. Brodsky, S.D. Glazek, X. Zhao, G. Chen, M. Gomez-Rocha, and S. Leitão. I also want to thank the hospitality of the High Energy Nuclear Theory Group at the Institute of Modern Physics, Chinese Academy of Sciences, Lanzhou, China, where the work is being completed. This work was supported in part by the Department of Energy under Grant Nos. DE-FG02-87ER40371 and DESC0008485 (SciDAC-3/NUCLEI). Computational resources were provided by the National Energy Research Supercomputer Center (NERSC), which is supported by the Office of Science of the U.S. Department of Energy under Contract No. DE-AC02-05CH11231.

A Derivation of Equations (10–11)

We used the identity:

$$\nabla_{q_\perp}^2 = \frac{\partial^2}{\partial q_\perp^2} + \frac{d-1}{q_\perp} \frac{\partial}{\partial q_\perp} + \frac{1}{q_\perp^2} L_z^2 = 4t \frac{\partial^2}{\partial t^2} + 2d \frac{\partial}{\partial t} + \frac{1}{t} L_z^2 \quad (12)$$

where $d = 2$ is the spatial dimension, and $t \equiv q_\perp^2$. The angular momentum operator $L_z = i\partial/\partial\phi$. The two-dimensional Laplacian has a different coefficient from the three-dimensional one, which results the factor $3/2$. At $t \rightarrow 0$, the first term $4t\partial^2/\partial t^2$ vanishes. The form factor does not have angle dependence, so, the third term vanishes as well. Then, at $t \rightarrow 0$,

$$\langle r^2 \rangle = -6 \frac{\partial}{\partial t} F(t) \Big|_{t \rightarrow 0} = -\frac{3}{2} \nabla_{q_\perp}^2 I_{\lambda\lambda'}(\mathbf{q}_\perp) \Big|_{q_\perp \rightarrow 0}, \quad (13)$$

where $I_{\lambda\lambda'}(\mathbf{q}_\perp)$ is the helicity amplitude. In the LFWF representation [19],

$$I_{\lambda\lambda'}^{\text{em}}(\mathbf{q}_\perp) = \sum_{s,s'} \int_0^1 \frac{dx}{2x(1-x)} \int \frac{d^2 k_\perp}{(2\pi)^3} \psi_{ss'/h}^{(\lambda')*}(\mathbf{k}_\perp + (1-x)\mathbf{q}_\perp, x) \psi_{ss'/h}^{(\lambda)}(\mathbf{k}_\perp, x), \quad (14)$$

$$I_{\lambda\lambda'}^{\text{gr}}(\mathbf{q}_\perp) = \sum_{s,s'} \int_0^1 \frac{dx}{2x(1-x)} \int \frac{d^2 k_\perp}{(2\pi)^3} \left[x \psi_{ss'/h}^{(\lambda')*}(\mathbf{k}_\perp + (1-x)\mathbf{q}_\perp, x) \psi_{ss'/h}^{(\lambda)}(\mathbf{k}_\perp, x) \right. \\ \left. + (1-x) \psi_{ss'/h}^{(\lambda')*}(\mathbf{k}_\perp - x\mathbf{q}_\perp, x) \psi_{ss'/h}^{(\lambda)}(\mathbf{k}_\perp, x) \right]. \quad (15)$$

Equations (10–11) immediately follow.

References

1. B.L.G. Bakker *et al.*, Nucl. Phys. Proc. Suppl. **251-252**, 165 (2014).
2. G.P. Lepage and S.J. Brodsky, Phys. Rev. D **22**, 2157 (1980).
3. Yang Li, P. Maris, X. Zhao, J.P. Vary, Phys. Lett. B **758**, 118 (2016).

-
4. G. Chen, Yang Li, P. Maris, K. Tuchin, J.P. Vary, arXiv:1610.04945 [nucl-th].
 5. T. Hilger, C. Popovici, M. Gomez-Rocha, and A. Krassnigg, Phys. Rev. D **91**, 034013 (2015).
 6. S. Leito, A. Stadler, M. T. Pea and E. P. Biernat, Phys. Lett. B **764**, 38 (2017).
 7. S.J. Brodsky, G.F. de Teramond, H.G. Dosch and J. Erlich, Phys. Rept. **584**, 1 (2015).
 8. David Griffiths, “Introduction to Elementary Particles”, 2nd revised ed., Wiley-VCH, ISBN: 978-3-527-40601-2
 9. M. Krautgärtner, H.C. Pauli, and F. Wölz, Phys. Rev. D **45**, 3755 (1992).
 10. H. Lamm, R.F. Lebed, J. Phys. G **41**, 125003 (2014).
 11. P. Wiecki, Yang Li, X. Zhao, P. Maris, J.P. Vary, Phys. Rev. D **91**, 105009 (2015).
 12. M. Mangin-Brinet, J. Carbonell, V.A. Karmanov, Phys. Rev. C **68**, 055203 (2003).
 13. D. Atkinson and P.W. Johnson, Phys. Rev. D **37**, 2296 (1988).
 14. H.W. Crater and J. Schiermeyer, Phys. Rev. D **82**, 094020. (2010); J.R. Spence, J.P. Vary, in preparation.
 15. S.D. Glazek, A. Harindranath, S.S. Pinsky, J. Shigemitsu, and K.G. Wilson, PhysRevD **47**, 1599 (1993); U. Trittmann and H.-C. Pauli, MPI H-V4-1997, arXiv:hep-th/9704215; D. Chakrabarti, and A. Harindranath. Phys. Rev. D **64**, 105002 (2001).
 16. M. Burkardt, Phys. Rev. D **62**, 071503 (2000), *Erratum: ibid.* **66**, 119903 (2002).
 17. M. Diehl, Phys. Rept. **388**, 41 (2003).
 18. L. Adhikari, Yang Li, X. Zhao, P. Maris, J.P. Vary, A.A. El-Hady, Phys. Rev. C **93**, 055202 (2016).
 19. S.J. Brodsky, D.S. Hwang, B. Ma and I. Schmidt, Nucl. Phys. B **593**, 311 (2001).
 20. V.A. Karmanov, J.-F. Mathiot, and A.V. Smirnov, Phys. Rev. D **69**, 045009 (2004).
 21. V.A. Karmanov, J.-F. Mathiot, and A.V. Smirnov, Phys. Rev. D **75**, 045012 (2007).
 22. V.A. Karmanov, J.-F. Mathiot, and A.V. Smirnov, Phys. Rev. D **77**, 085028 (2008).
 23. Li, Yang, V.A. Karmanov, P. Maris, J.P. Vary, Phys. Lett. B **748**, 278 (2015).
 24. For example: J.P. Vary, *et. al.*, Phys. Rev. C **81**, 035205 (2010); S.S. Chabysheva, J.R. Hiller, Phys. Lett. B **711**, 417 (2012).
 25. For example: M. Gómez-Rocha and S.D. Glazek Phys. Rev. D **92**, 065005 (2015); E.L. Gubankova and F. Wegner, Phys. Rev. D **58**, 025012 (1998).